Computational Materials Science II

Progress Report # 5

Vourvachakis S. Georgios
mse354

May 10, 2025

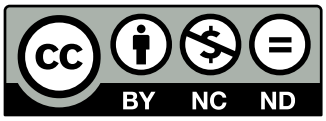

Contents

1

Introduction

Density-functional theory (DFT) provides a first-principles framework for computing the vibrational properties of solids and molecules [1],[2],[3]. Vibrational phenomena have a long history: Einstein first modeled a crystal as quantized harmonic oscillators (1907) and Debye (1912) introduced collective acoustic modes to explain heat capacity [4]. In modern terms, small oscillations of atoms about their equilibrium positions are described by phonons, the quantized normal modes of the lattice.

Even at absolute zero each mode has a zero-point energy, so atoms vibrate quantum-mechanically in the ground state. In the *harmonic approximation* one expands the potential energy around equilibrium: for a single displacement coordinate x we write

$$V(x_0 + \delta) \approx V_0 + \frac{1}{2}\delta^2 \frac{d^2V}{d\delta^2}\Big|_{\delta=0},$$

with $\delta = x - x_0$ and $V_0 = V(x_0)$.

In multiple dimensions one obtains a Taylor expansion given $\mathbf{q} \in \mathbb{R}^N$ generalized coordinates of the oscillators:

$$V(\mathbf{q}_0 + \boldsymbol{\delta}) \approx V_0 + \frac{1}{2}\sum_{ij} \frac{\partial^2 V}{\partial q_i \partial q_j}\Big|_{\mathbf{q}_0} \delta_i \delta_j \equiv V_0 + \boldsymbol{\delta}^\top H_V(\mathbf{q})\boldsymbol{\delta},$$

so the energy is a quadratic form in the displacements. This Hessian matrix of second derivatives, $H_V(\mathbf{q})$, defines a set of uncoupled harmonic oscillators (*normal modes*). In DFT one computes $V_{(BO)}$ (the Born–Oppenheimer energy) as a function of atomic positions and uses finite differences or perturbation theory to obtain the force-constant matrix [phonons in ASE],[4]. Vibrational frequencies (ω) then follow from the eigenvalues of this Hessian divided by the masses. These DFT-calculated phonon energies can be directly compared with experimental infrared or Raman spectra [5],[6].

1.1 Vibrational Modes in Diatomic Molecules

For a diatomic molecule A–B of masses m_A, m_B bound by an (approximately) harmonic potential, the classical equation of motion yields a single stretching mode. Denoting the displacement from equilibrium by δ, Hooke's law gives $\mathbf{F} = -k\delta$ with (isotropic) spring constant k.

Introducing the reduced mass

$$\mu = \left(\frac{1}{m_A} + \frac{1}{m_B}\right)^{-1},$$

one finds a harmonic oscillator with angular frequency $\omega = \sqrt{k/\mu}$ and ordinary frequency $\nu = \omega/(2\pi)$. Thus $\nu = \frac{1}{2\pi}\sqrt{\frac{k}{\mu}}$.

In quantum mechanics the vibrational energy levels are $E_n = E_0 + (n + \frac{1}{2})h\nu$, so the fundamental transition has energy $E = h\nu$. Vibrational energies are often expressed in electron-volts or as wavenumbers ($\tilde{\nu} = 1/\lambda$ in cm^{-1}); for reference $1\mathrm{eV} \approx 8065.5\mathrm{cm}^{-1}$.

In practice, we compute diatomic frequencies with DFT by displacing one atom by a small δ (e.g. 0.05–0.1Å) and calculating the resulting force or energy change. A finite-difference fit yields the effective $k = d^2E/d\delta^2$ [phonons in ASE], from which ν follows.

For example, we will apply this to carbon monoxide (CO) and hydrogen chloride (HCl), each having one stretching mode (e.g., the GPAW tutorial notes that "for a simple molecule, like CO, there is only one stretching mode" which makes intuitive sense). The computed frequencies from GPAW/ASE can then be compared to experimental values[1].

1.2 Normal Modes of Polyatomic Molecules

For a molecule of N atoms ($3N$ total Cartesian degrees of freedom), rigid translations and rotations do not change the energy. Thus a nonlinear molecule has $3N - 6$ vibrational modes (degrees of freedom), while a linear molecule has $3N - 5$. In the harmonic approximation, the potential energy surface near the equilibrium $\mathbf{q}_0$ is quadratic in the $3N$ displacements. Defining the Hessian $H_{ij} \coloneqq \left.\frac{\partial^2 E}{\partial q_i \partial q_j}\right|_{\mathbf{q}_0}$, the vibrational normal modes are given by the eigenvectors of the mass-weighted Hessian. The classical potential energy is $E = E_0 + \frac{1}{2}k\delta^2$ for each mode, whereas the quantum levels are $E_n = E_0 + (n + \frac{1}{2})h\nu$, $n \in \mathbb{N}$.

In computational practice one first optimizes the geometry (e.g. with a Quasi-Newton minimizer) and then constructs the Hessian by small displacements of each atom. The ASE `Vibrations` module automates this: it displaces atoms, computes forces or energies with GPAW, and diagonalizes the force-constant matrix to yield all $3N - 6$ (or $3N - 5$) nonzero frequencies. The GPAW tutorial for H_2O illustrates this workflow: it builds the molecule, optimizes it, and then calls `Vibrations(h2o).run()`, finally printing the mode frequencies and eigenvectors. We will follow this example for water and other polyatomics.[2]

[1] The Vibrations tutorial demonstrates the same procedure on H_2O and suggests the analogous approach for diatomics.

[2] For a more thorough description of normal modes and its degrees of freedom the reader is referred to the LibreTexts' (Chemistry Library) description on Vibrational Modes.

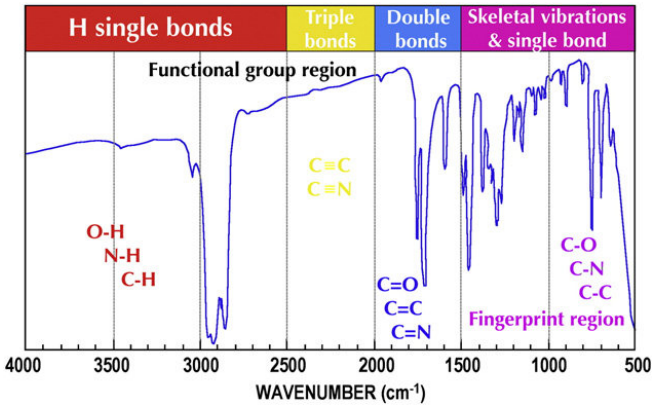

Figure 1: A typical mid-IR transmission spectrum with typical absorptions lines associated to vibrational modes of molecules, organic components and others contributions of biological and non-biological nature.[7]

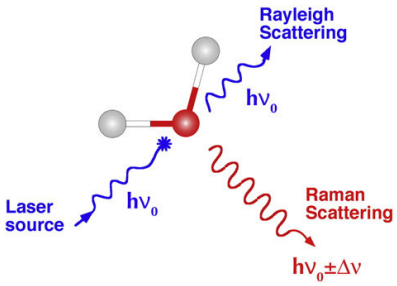

Figure 2: Layout of light scattering processes with a molecule: Rayleigh scattering (green) and anti-Stokes Raman scattering (red).[7]

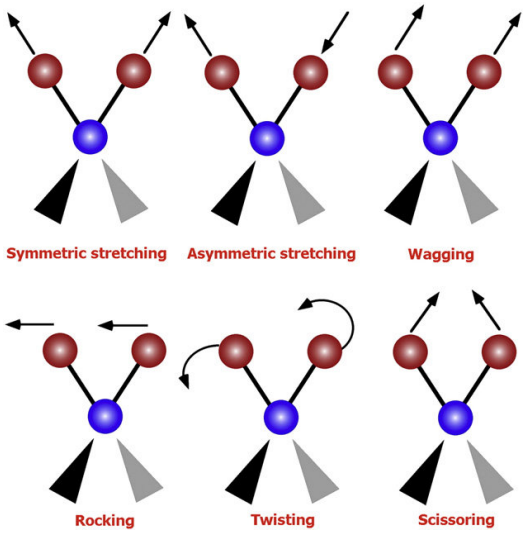

Figure 3: Vibrational modes associated to a molecular dipole moment change detectable in an IR absorption spectrum. In addition to the two stretching modes, the four different bending vibrations are depicted.[7]

1.3 Lattice Vibrations and Band Formation in Crystals

We begin by formulating the 1D monatomic chain in a Lagrangian framework, derive its equations of motion, and—by invoking Bloch's theorem—prove that the normal-mode solutions

$$u_n(q,t) = Ae^{i(nqa-\omega t)}$$

satisfy

$$\omega^2(q) = \omega_0^2 + \frac{4C}{m}\sin^2\left(\frac{qa}{2}\right)$$

Extending to a diatomic basis leads to a 2×2 eigenvalue problem and yields both acoustic and optical branches. In three dimensions, the dynamical matrix formalism generalizes these results, predicting 3p phonon bands for p atoms per unit cell. We also discuss non-analytic corrections (LO–TO splitting) in polar crystals, and outline how first-principles codes (e.g. GPAW+ASE) construct and diagonalize the dynamical matrix to compute full phonon band structures.

1.3.1 Monatomic 1D Chain

Consider identical atoms (mass m) on a 1D lattice with spacing a, each coupled to nearest neighbors by isotropic springs of constant C and subject to on-site restoring frequency ω_0. The Lagrangian is

$$\mathcal{L} = \sum_n \left[\frac{1}{2}m\dot{u}_n^2 - \frac{1}{2}C(u_{n-1}-u_n)^2 - \frac{1}{2}m\omega_0^2 u_n^2\right] .$$

Let $\mathcal{P}(a,b,\mathbf{x}_a,\mathbf{x}_b)$ be the set of smooth paths $\mathbf{q} : [a,b] \mapsto X$ for which $\mathbf{q}(a) = \mathbf{x}_a$ and $\mathbf{q}(b) = \mathbf{x}_b$. The *action functional* $S : \mathcal{P}(a,b,\mathbf{x}_a,\mathbf{x}_b) \mapsto \mathbb{R}$ is defined via

$$S(\mathbf{q}) \coloneqq \int_a^b \mathcal{L}(t,\mathbf{q}(t),\dot{\mathbf{q}}(t))dt .$$

A path $\mathbf{q} \in \mathcal{P}(a,b,\mathbf{x}_a,\mathbf{x}_b)$ is a stationary point[3] of S if and only if

$$\frac{\partial\mathcal{L}}{\partial q^n}(t,\mathbf{q}(t),\dot{\mathbf{q}}(t)(t)) - \frac{d}{dt}\frac{\partial\mathcal{L}}{\partial\dot{q}^n}(t,\mathbf{q}(t),\dot{\mathbf{q}}(t)) = 0 , \; n = 1,\ldots,N$$

where N are the degrees of freedom of an $(X,\mathcal{L})$ dynamical system[4].

In our case of N uncoupled oscillators (each one having one degree of freedom, the oscillation amplitude), we obtain from the *Euler-Lagrange* equation above ($[N] = 1,\ldots,N$):

$$m\ddot{u}_n = -C(2u_n - u_{n-1} - u_{n+1}) - m\omega_0^2 u_n , \; \forall n \in [N]$$

[3] We refer to a stationary point of S with respect to any small perturbation in $\mathbf{q}$, i.e. $\mathbf{q} = \mathbf{q}_0 + \epsilon\delta\boldsymbol{\eta}$ for $\epsilon \ll 1$, where $\delta\mathbf{q} \equiv \epsilon\delta\boldsymbol{\eta}$ is the *variation* of $\mathbf{q}_0$ with $\delta\boldsymbol{\eta}$ an arbitrary function that has at least one derivative and vanishes at the endpoints ($\delta\boldsymbol{\eta}(a) = \delta\boldsymbol{\eta}(b) = 0$).

[4] X denotes the configurational space and $\mathcal{L} = \mathcal{L}(t,\mathbf{q}(t),\dot{\mathbf{q}}(t))$ the Lagrangian.

Assume the Bloch-wave ansatz:

$$u_n(q,t) = Ae^{i(nqa-\omega t)} .$$

Substituting into the above EOM yields

$$-m\omega^2 e^{i(nqa-\omega t)} = -C(2 - e^{-iqa} - e^{iqa})e^{i(nqa-\omega t)} - m\omega_0^2 e^{i(nqa-\omega t)} \Longrightarrow$$
$$\omega^2 = \omega_0^2 + \frac{C}{m}[2 - 2\cos(qa)] = \omega_0^2 + \frac{4C}{m}\sin^2\left(\frac{qa}{2}\right) ,$$

proving the dispersion relation. □

Because the ansatz satisfies the linear EOM, the general solution is a superposition of modes:

$$u_n(t) = \sum_q [A_q e^{i(nqa-\omega(q)t)} + A_{-q}e^{-i(nqa-\omega(q)t)}] \equiv \sum_q [A_q e^{i(nqa-\omega(q)t)} + c.c] .$$

The periodicity $\omega(q) = \omega(q + 2\pi/a)$ confines q to the first Brillouin zone (Fig. 4).

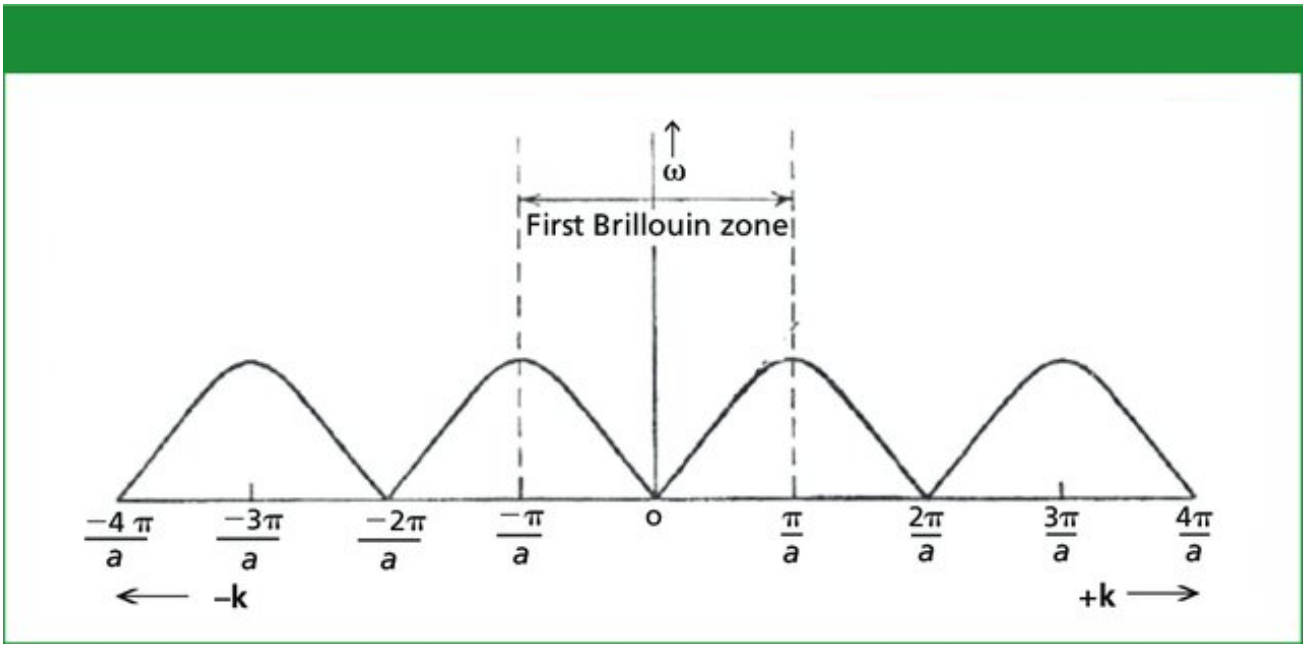

Figure 4: Phonon dispersion curve for a linear monatomic lattice.[8]

1.3.2 Diatomic 1D Chain: Acoustic and Optical Branches

Two atoms per cell (masses m_1,m_2) connected by springs C. Let displacements $u_{n,1}$, $u_{n,2}$ in cell n.

The equations

$$\begin{cases} m_1\ddot{u}_{n,1} = -C(2u_{n,1} - u_{n,2} - u_{n-1,2}), \\ m_2\ddot{u}_{n,2} = -C(2u_{n,2} - u_{n,1} - u_{n+1,1}), \end{cases}$$

assume $u_{n,a} \propto e^{i(nqa-\omega t)}$ and form a 2×2 eigenvalue problem $D(q)\mathbf{e} = \omega^2 M\mathbf{e}$ (see page 10 in Cornell's ECE407 lecture slides).

Its two eigenvalues yield:

- Acoustic branch $\omega_{\text{ac}} \to 0$ as $q \to 0$.
- Optical branch $\omega_{\text{op}} > 0$.

See detailed derivation and dispersion plot-animation from Graz Center of Physics.

1.3.3 Dynamical Matrix in 3D and Phonon Count

In d dimensions with direct lattice basis $\{\boldsymbol{\alpha}\}$, displacements are of the form

$$u_\alpha(\mathbf{R}_\ell, t) \propto e^{i(\mathbf{q}\cdot\mathbf{R}_\ell - \omega t)}\mathbf{e}_\alpha(\mathbf{q}) \,,$$

with $\mathbf{R}_\ell = \ell_1\alpha_1 + \ell_2\alpha_2 + \ell_3\alpha_3 \equiv \boldsymbol{\ell}\cdot\boldsymbol{\alpha}$, the direct lattice translation vector.

In comparison with the 1D chain analysis above, the *dynamical matrix* is

$$D_{\alpha\beta}(\mathbf{q}) = \sum_{\mathbf{R}'} \Phi_{\alpha\beta}(\mathbf{o}, \mathbf{R}')e^{i\mathbf{q}\cdot\mathbf{R}'} \,,$$

where the one-form (or covector field) $\Phi : \mathbb{R}^d \times \mathbb{R}^d \mapsto \mathbb{R}$ denotes force constants. Diagonalizing $D(\mathbf{q})$ gives $3p$ bands for p atoms in the primitive unit cell: 3 acoustic, $3p-3$ optical.

Long-range Coulomb interactions add a non-analytic term at Γ, splitting longitudinal/transverse optic modes. This is captured by a correction to $D(\mathbf{q})$ as $\mathbf{q} \to \mathbf{o}$, leading to the *Lyddane–Sachs–Teller relation* $\omega_{LO}^2/\omega_{TO}^2 = \epsilon_\infty/\epsilon_0$ (see the Physics Stack Exchange's discussion in LO-TO splitting)[9]. Indicatively, we depict the Germanium's (Ge) phonon dispersion in Figure 5.

1.3.4 First-Principles Phonon Calculations

Codes like ASE and GPAW use small displacements $\pm\delta$ in a large N^3 supercell to compute forces, build Φ, then Fourier transform to obtain $D(\mathbf{q})$ and $\omega(\mathbf{q})$.

In DFT one computes the phonon band structure by generating the dynamical matrix (Fourier transform of the force constants, Φ,) and diagonalizing at each $\mathbf{q}$-point. The most direct approach is the finite-displacement (supercell) method: one builds a large N^3 supercell, displaces each atom by $\pm\delta$, computes forces (or energies) with GPAW, and extracts the force-constant matrix $D(\mathbf{q})$. However, this is computationally expensive for large cells [10]. An alternative is to invoke empirical interatomic potentials (such as the *Effective Medium Theory*, EMT) to estimate phonons cheaply [11].

In this assignment, we carry out a first-principles phonon calculation for aluminum. Specifically, we compute the phonon band structure of FCC Al using GPAW and the ASE `Phonons` class (see the ASE/GPAW phonon tutorial) which calculates the phonon dispersion for bulk aluminum using a $7\times7\times7$ supercell within effective medium theory. This involves creating a sufficiently large supercell, using the finite-displacement

method to obtain the dynamical matrix, and finally plotting $\omega(\mathbf{q})$ along high-symmetry directions in the Brillouin zone. By comparing with known results (e.g. Debye model or experimental inelastic neutron data), one gains insight into lattice dynamics from a DFT perspective.

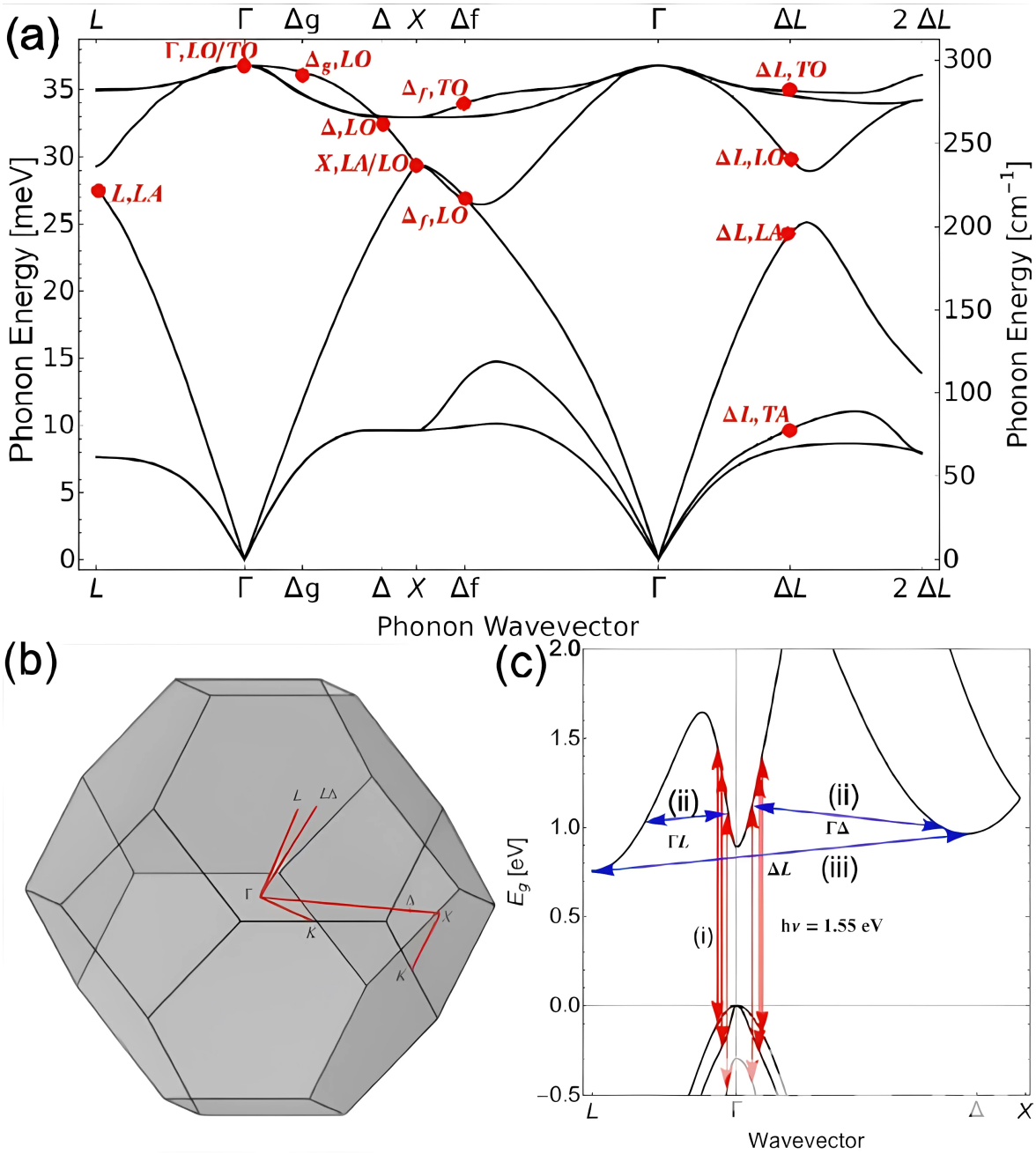

Figure 5: (a) Phonon dispersion of Ge. The phonons generated by electron–phonon coupling (EPC) are depicted in red circles. (b) First Brillouin zone of Ge. The red lines show directions of interest. Note that the LΔ phonons, generated by the L → Δ transition, occur very close to the L point in the Brillouin zone. (c) Electronic band structure of Ge. The vertical red arrows show the initial optical excitation transitions across the band-gap possible with a 1.55 eV pump pulse. The blue arrows show the transitions between the Γ, Δ, and L valleys that generate the non-equilibrium phonon population.[12]

2

Results and Remarks

Here we outline the scope of our computational vibrational analysis, which proceeds in three stages. First, we determine the fundamental stretching frequencies of CO and HCl by applying finite displacements of $\delta \in \{0.05, 0.1\}$Å about their DFT-optimized equilibrium bond lengths, following the procedure in the GPAW/ASE Vibrations tutorial. In this approach, the energy change $\Delta E(\delta)$ is fitted to extract the effective spring constant $k = d^2E/d\delta^2$, yielding the vibrational frequency $\nu = \frac{1}{2\pi}\sqrt{k/\mu}$ with the reduced mass μ of the diatomic pair. The computed frequencies are then benchmarked against experimental gas-phase values. Next, we compute all $3N - 6$ vibrational modes of H_2O by first optimizing its geometry with ASE's `QuasiNewton` optimizer and then running the ASE Vibrations module within GPAW to obtain eigenfrequencies and eigenvectors, as illustrated in the GPAW Vibrations tutorial. Finally, we construct the phonon band structure of FCC Al using the ASE `Phonons` class with the Effective Medium Theory (EMT) potential in a $7 \times 7 \times 7$ supercell, performing finite displacements $\delta = 0.05$Å to assemble the real-space force-constant matrix and Fourier-transform it to obtain $\omega(\mathbf{q})$ along high-symmetry paths.

This workflow—from simple diatomics through polyatomic molecules to extended solids—demonstrates the consistency and flexibility of the ASE/GPAW framework for vibrational analyses across chemical length scales.

2.1 Diatomic Vibrational Analysis on CO and HCl

In this study, we determined the fundamental stretching frequencies of CO and HCl by displacing each diatomic molecule symmetrically about its DFT-optimized bond length using $\delta = 0.05$Å and $\delta = 0.10$Å, fitting the resulting $E(\delta)$ curve to a harmonic potential, and extracting the force constant k. From k and the reduced mass μ we computed the vibrational frequency $\nu = \frac{1}{2}\sqrt{k/\mu}$. For CO, the 0.10Å displacement yielded $\nu \approx 1976.2$ cm^{-1} (7.8 % low), while the 0.05Å displacement gave 1950.4 cm^{-1} (9.0 % low) compared to the experimental[5]. For HCl, the corresponding values were 2906.3 cm^{-1} (0.7 % high) and 2882.5 cm^{-1} (0.1 % low) versus the experimental[6] 2886.0 cm^{-1}. These results demonstrate that smaller displacements improve harmonic fitting for light-atom diatomics and confirm the reliability of GPAW/ASE finite-difference workflows for simple molecules.

[5] Measured by Infrared Absorption Spectroscopy (IR). By the Coblentz Society, then compiled in the NIST Chemistry WebBook 2143 cm^{-1} which then cites the work by Huber et al. (1979) [13].

[6] Measured by IR. By the Coblentz Society, then compiled in the NIST Chemistry WebBook which in turn cites the work by Benedict et al. (1956) [14].

Table 1: Comparison of Calculated and Experimental Vibrational Properties for CO and HCl Molecules

Fundamental Vibrational Frequency ($v = 1 \leftarrow v = 0$)				
Property	**CO**		**HCl**	
	Displacement (-0.1, 0.1)	**Displacement (-0.05, 0.05)**	**Displacement (-0.1, 0.1)**	**Displacement (-0.05, 0.05)**
Calculated frequency (cm^{-1})	1976.19	1950.37	2906.28	2882.49
Experimental frequency (cm^{-1})	2143.00	2143.00	2886.00	2886.00
Difference (cm^{-1})	166.81	192.63	20.28	3.51
Relative difference (%)	7.78	8.99	0.70	0.12
Equilibrium bond length (Å)	1.1579	1.1579	1.2935	1.2935
Experimental Values				
Energy (eV)	-10.35		-5.95	
Bond length (Å)	1.22		1.27	
PBE Energy Minimum				
Energy (eV)	-10.52		-5.96	
Bond length (Å)	1.16		1.29	
Calculated Force Constants				
Force constant (eV/Å^2)	98.5272	95.9691	30.4439	29.9475
Force constant (N/m)	1.5786×10^3	1.5376×10^3	4.8776×10^2	4.7981×10^2
Calculated Vibrational Properties				
Frequency (Hz)	5.9245×10^{13}	5.8471×10^{13}	8.7128×10^{13}	8.6415×10^{13}

2.1.1 Computational Workflow

We modeled each diatomic (CO or HCl) in a large cubic cell (10Å per side) to minimize image interactions, placing atoms at $\pm d/2$ around the cell center, where d is the experimental bond length (1.22Å for CO and 1.27Å for HCl). After a single-point DFT calculation (PBE, plane-wave basis, RMM-DIIS solver), we performed a QuasiNewton relaxation (force criterion $fmax = 0.01eV/$Å) to obtain the equilibrium bond length d_0 and total energy E_0.

Around d_0, we generated 11 points spanning $\delta \in [-p, p]$ with $p = 0.05$Å and 0.10Å. At each displacement we computed the DFT energy $E(\delta)$ and fitted to

$$E(\delta) = E_0 + \frac{1}{2}k\delta^2$$

to extract the effective spring constant $k = d^2E/d\delta^2$. The reduced mass μ for CO and HCl was calculated via equation 1.1, with atomic masses from standard tables, allowing the vibrational frequency ν to be determined in Hz and converted to wavenumbers (cm^{-1}) by $\tilde{\nu} \approx \nu/(c \cdot 100)$, where c is the speed of light in vacuum.

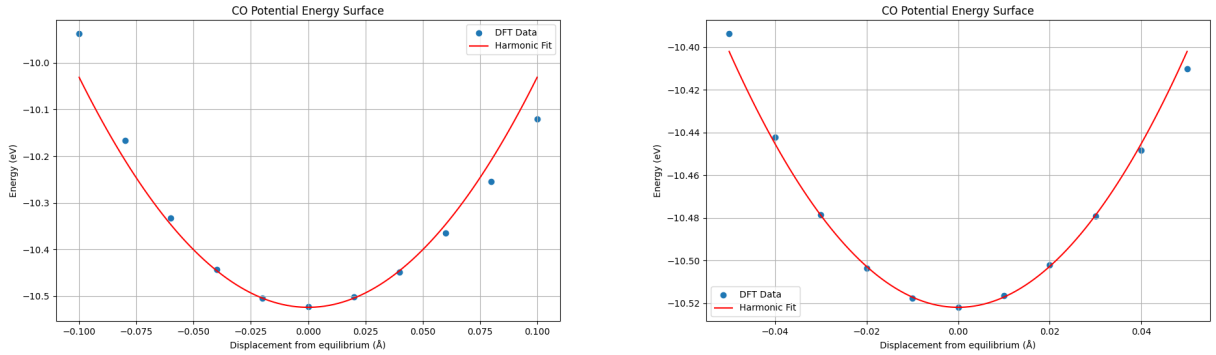

Figure 6: Plots of calculated potential energy for different displacements, $\delta = 0.1$Å (left) and $\delta = 0.05$Å (right) for a single CO molecule.

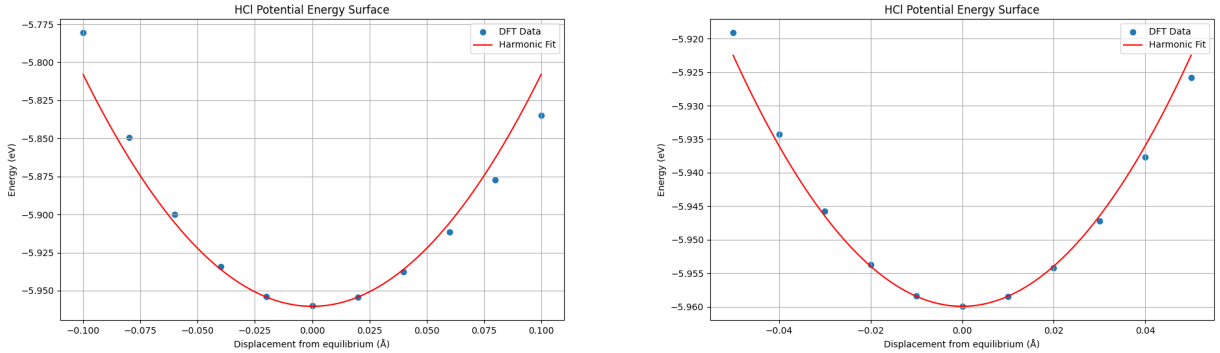

Figure 7: Plots of calculated potential energy for different displacements, $\delta = 0.1$Å (left) and $\delta = 0.05$Å (right)for a single HCl molecule.

The comparative analysis shows that smaller displacement amplitudes yield slightly better harmonic fits, particularly for lighter diatomics like HCl, where anharmonic contributions at larger δ are more pronounced. The systematic underestimation for CO indicates functional-dependent errors in PBE and highlights the importance of benchmarking against experiment and choosing appropriate δ ranges when extracting force constants in DFT workflows.

2.2 Normal Modes of Water Molecule

We optimized the geometry of the H_2O molecule using ASE's `QuasiNewton` optimizer in conjunction with GPAW, then computed all $3N - 6 = 3$ ($N = 3$) vibrational modes via the ASE Vibrations module, obtaining eigenfrequencies and eigenvectors that correspond to the bending, symmetric stretch, and antisymmetric stretch modes. The calculated frequencies were compared to the experimental gas-phase values of 1595 cm^{-1}

(bending), 3657 cm^{-1} (symmetric stretch), and 3756 cm^{-1} (antisymmetric stretch) to assess accuracy and potential error sources such as basis set limitations and anharmonicity.

The vibrational spectrum in DFT is derived from the potential energy surface's second derivatives, but a complete quantum description entails solving the time-dependent Schrödinger equation for nuclear motion,

$$i\hbar\frac{\partial\Psi(\{\mathbf{R}\},t)}{\partial t} = \mathcal{H}(\{\mathbf{R}\})\Psi(\{\mathbf{R}\},t)\,,$$

where $\{\mathbf{R}\}$ are the nuclear coordinates and $\mathcal{H}$ includes both kinetic and potential terms of all atoms.

For dynamic visualization, users can execute the provided `h2o_viz.py` module to generate movies of the bending, symmetric, and antisymmetric modes from the `vib._.traj` files produced by ASE.

2.2.1 Computational Procedure

We constructed an H_2O molecule with O-H bond length $d = 0.9575$Å and H–O–H angle 104.51°, centered in a vacuum box with 3.5Å padding to eliminate spurious interactions. The GPAW calculator was configured in LCAO mode with a double-ζ polarized (`dzp`) basis and PBE exchange–correlation, with symmetry disabled to capture all modes accurately. Then, geometry optimization was performed until the maximum force $f_{\max} \leq 0.05 eV/$Å, ensuring an accurate equilibrium structure for vibrational analysis. The ASE `Vibrations` object was instantiated and run to compute the full set of $3N = 9$ modes, of which six are translations and rotations (including small imaginary modes due to numerical noise) and three are true vibrations. Finally, frequencies and eigenvectors were obtained via `vib.summary(method='frederiksen')`, and mode trajectories were written to files `vib.0.traj` through `vib.8.traj` for visualization with ASE GUI or other molecular viewers.

Table 2: Vibrational Analysis Summary

Mode	Energy (meV)	Wavenumber (cm^{-1})	Description
0	$51.3i$	$413.9i$	Imaginary frequency
1	$40.6i$	$327.5i$	Imaginary frequency
2	$23.1i$	$186.6i$	Imaginary frequency
3	$0.8i$	$6.2i$	Imaginary frequency
4	5.6	45.5	Real vibrational mode
5	9.0	72.7	Real vibrational mode
6	186.9	1507.3	Real vibrational mode
7	450.7	3635.2	Real vibrational mode
8	465.0	3750.8	Real vibrational mode
Zero-point energy: 0.559 eV			

From the above table we notice four imaginary frequencies (modes 0-3), which typically indicate a transition state or unstable geometry in the molecular structure, five real vibrational modes (modes 4-8), with

frequencies ranging from low (45.5 cm^{-1}) to high (3750.8 cm^{-1}). The highest frequency modes (7 and 8) are likely stretching vibrations, while the mid-range frequency (mode 6) could be a bending mode.

The presence of multiple imaginary frequencies suggests this is a higher-order saddle point rather than a simple transition state (which would typically have just one imaginary frequency).

2.3 Aluminum Phonon Dispersion

We constructed the phonon band structure of face-centered cubic (FCC) aluminum using the small-displacement (finite-difference) method implemented in ASE's `Phonons` class with the Effective Medium Theory (EMT) potential on a $7 \times 7 \times 7$ supercell. By displacing each atom by $\delta = 0.05$Å in all independent directions, we compute the force-constant matrix

$$\Phi_{i\alpha,j\beta} \coloneqq \frac{\partial^2 E}{\partial R_{i\alpha} \partial R_{j\beta}} ,$$

by finite differences: displacing atom j in direction β and evaluating forces on atom i in direction α. The dynamical matrix at wavevector $\mathbf{q}$ is then

$$D_{\alpha\beta}(\mathbf{q}) \coloneqq \frac{1}{\sqrt{m_\alpha m_\beta}} \sum_{\ell'} \Phi_{a\mathbf{0},\beta\ell'} e^{i\mathbf{q}\cdot\mathbf{R}_{\ell'}} ,$$

where m_α are atomic masses and $\mathbf{R}_{\ell'}$ lattice translation vectors.

Then the eigenvalue problem

$$\det|D(\mathbf{q}) - \omega^2 I| = 0 \Leftrightarrow \sum_\beta D_{\alpha,\beta}(\mathbf{q}) e_\beta^{(\nu)}(\mathbf{q}) = \omega_\nu^2(\mathbf{q}) e_\alpha^{(\nu)}(\mathbf{q}) , \forall \text{ branch } \nu$$

is solved to obtain phonon frequencies $\omega_\nu(\mathbf{q})$ for each ν branch along high-symmetry paths and the phonon density of states (DOS) [15].

The resulting dispersion exhibits three acoustic branches that go to zero at Γ, no optical branches (monatomic basis), and minor imaginary modes at Γ ($\sim 10^{-8} i$ THz) attributable to numerical noise.

The phonon spectrum peaks near $\omega \approx 0.035$ eV (~ 280 cm^{-1}) , in good qualitative agreement with literature EMT calculations for Al (see Fig. 9 for a more precise band structure calculation)[7].

After running `ph.run()` to compute and store forces, we invoked

```
ph.read(acoustic=True)
ph.clean()
```

to assemble and symmetrize the dynamical matrix (including enforcing acoustic sum rules) and then generated a band path 'GXULGK' over 100 q-points via `atoms.cell.bandpath('GXULGK',npoints=100)`.

[7] Inelastic-neutron and anharmonic-broadening measurements corroborate this, reporting a broader DOS peak near 37 meV (~ 298 cm^{-1}) for Al at elevated temperatures, attributable predominantly to LA-branch phonons near zone-boundary points [16].

The phonon band structure $\omega(\mathbf{q})$ was plotted alongside the phonon DOS, obtained by sampling a 20×20×20 q-grid with Gaussian broadening (width of 1 meV), showing the characteristic acoustic branches and no optical branches for monatomic Al.

As aluminum is non-polar, no non-analytical LO–TO correction at Γ is required; ASE's current small-displacement implementation does not include polar splitting (see Yung Ting Lee's slides on phonon dispersion with LO-TO splitting for polar materials).

Overall, the workflow demonstrates that ASE's `Phonons` class with EMT can efficiently reproduce qualitative phonon band features of FCC Al. For quantitative DFT-level accuracy, one would replace EMT with a first-principles calculator (e.g., GPAW) and exploit crystal symmetries to reduce computational effort.

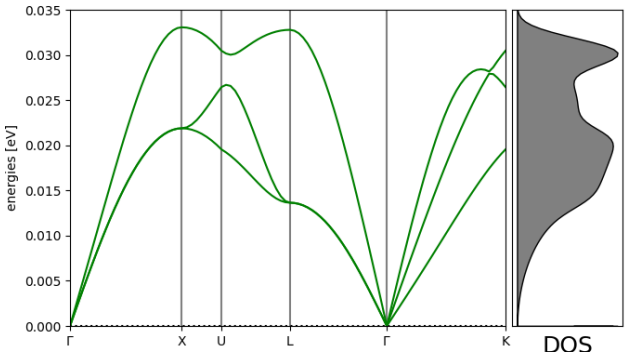

Figure 8: Phonon dispersions and DOS of FCC Al calculated with the small displacement (finite-difference) method using ASE's `Phonons` class with the EMT empirical potential.

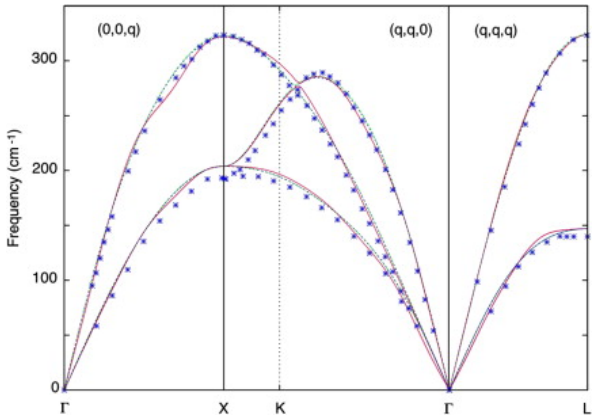

Figure 9: Phonon dispersions of Al calculated with the small displacement method and with linear response. Green and blue dashed lines (indistinguishable) correspond to calculations with a $4 \times 4 \times 4$ super-cell (small displacement) and a $4 \times 4 \times 4$ equispaced grid of q-points (linear response). Red and purple lines (indistinguishable) correspond to calculations with a $8 \times 8 \times 8$ super-cell and a $8 \times 8 \times 8$ grid of q-points with the two methods respectively. A small difference can be noticed between the $4 \times 4 \times 4$ and the $8 \times 8 \times 8$ sets, but no difference can be observed between the small displacement and the linear response methods. Experimental data are displayed with blue crosses, and are taken from Stedman et al. (1966) [17]. [15]

3 Environment Setup

This reference guide specifies user-dependent components of Python codes for performing Density Functional Theory (DFT) calculations using the GPAW (Grid-based Projector Augmented Wave method) software package and ASE (Atomic Simulation Environment).

The codes are organized in the directory `HW_5_codes` after `tag.gz` compression. The sub-directory `HW_5_codes/results` includes some indicative computational results of plots, `txt` and `traj` files (with sub-directories `CO_analysis` and `HCl_analysis` summarizing the experiments of the subsection 2.1).

In general, one can reproduce and verify the validity of the experiments across the report, given the appropriate resources for manageable execution time and version GPAW ≥ 25.1.0, and play around with alternative more accurate setups discussed in the respective sections.

Remark 3.1. Modules `h2o.py` and `diatomic_vib.py` require a proper GPAW (and thus ASE) environment setup (the others rely on ASE). Before running any calculation, users must modify the path settings to match their local installation.

The following function is introduced in the modules `h2o.py` and `diatomic_vib.py`, and requires user-specific modifications:

```
def setup_gpaw_paths(): # routine for gpaw setting
    # Suppress detailed GPAW output
    os.environ['GPAW_VERBOSE'] = 'o'
    sys.stdout = open(os.devnull, 'w')  # Redirect standard output

    # Clear existing paths and set the new one [user-dependent]
    intended_path = os.path.expanduser("~/Desktop/DFT_codes/gpaw_datasets"
    "/gpaw-setups-0.9.20000")
    setup_paths[:] = [intended_path]  # Replace all existing paths
    os.environ['GPAW_SETUP_PATH'] = intended_path

    sys.stdout = sys.__stdout__  # Restore standard output
    print("GPAW looking for datasets in:", setup_paths)
    print("Environment GPAW_SETUP_PATH:", os.environ['GPAW_SETUP_PATH'])
```

3.1 Adjusting the Path Settings

Users must update the `intended_path` variable to match their local GPAW dataset installation:

1. Locate your GPAW setups directory (typically installed with GPAW or downloaded separately).
2. Replace `'~/Desktop/DFT_codes/gpaw_datasets/gpaw-setups-0.9.20000'` with the path to your setups directory.

3. Ensure the path format is appropriate for your operating system:
    - Linux/macOS: Use `'/path/to/gpaw-setups'` .
    - Windows: Use `'C:/path/to/gpaw-setups'` or `r'C:\path\to\gpaw-setups'` .

References

[1] W. Kohn and L. J. Sham. "Self-Consistent Equations Including Exchange and Correlation Effects". In: *Phys. Rev.* 140 (4A Nov. 1965), A1133–A1138. DOI: 10.1103/PhysRev.140.A1133. URL: https://link.aps.org/doi/10.1103/PhysRev.140.A1133.

[2] D.S. Sholl and J.A. Steckel. *Density Functional Theory: A Practical Introduction*. Wiley, 2011. ISBN: 9781118211045. URL: https://books.google.gr/books?id=_f994dmAdv0C.

[3] Eric Cancès et al. "Numerical stability and efficiency of response property calculations in density functional theory". In: *Letters in Mathematical Physics* 113.1 (Feb. 2023). ISSN: 1573-0530. DOI: 10.1007/s11005-023-01645-3. URL: http://dx.doi.org/10.1007/s11005-023-01645-3.

[4] Mikhail Shubin and Toshikazu Sunada. "Geometric Theory of Lattice Vibrations and Specific Heat". In: *arXiv* (2006). eprint: math-ph/0512088 (math-ph). URL: https://arxiv.org/abs/math-ph/0512088.

[5] O.V. Bokotey et al. "First-principles calculations of phonons and Raman spectra in the Hg3Te2Cl2 crystals". In: *Journal of Alloys and Compounds* 669 (2016), pp. 161–166. ISSN: 0925-8388. DOI: https://doi.org/10.1016/j.jallcom.2016.02.005. URL: https://www.sciencedirect.com/science/article/pii/S0925838816302729.

[6] Ruth Pulido et al. "Phonon Structure, Infra-Red and Raman Spectra of Li2MnO3 by First-Principles Calculations". In: *Materials* 15.18 (2022). ISSN: 1996-1944. DOI: 10.3390/ma15186237. URL: https://www.mdpi.com/1996-1944/15/18/6237.

[7] Cyril Petibois et al. "Infrared Synchrotron sources - a boon for biology". In: *Nature Photonics* 3 (Jan. 2009).

[8] David Tuschel. "Why are the Raman spectra of crystalline and amorphous solids different?" In: 32 (Mar. 2017), pp. 26–33.

[9] R. H. Lyddane, R. G. Sachs, and E. Teller. "On the Polar Vibrations of Alkali Halides". In: *Phys. Rev.* 59 (8 May 1941), pp. 673–676. DOI: 10.1103/PhysRev.59.673. URL: https://link.aps.org/doi/10.1103/PhysRev.59.673.

[10] Martin H. Müser, Sergey V. Sukhomlinov, and Lars Pastewka and. "Interatomic potentials: achievements and challenges". In: *Advances in Physics: X* 8.1 (2023), p. 2093129. DOI: 10.1080/23746149.2022.2093129. eprint: https://doi.org/10.1080/23746149.2022.2093129. URL: https://doi.org/10.1080/23746149.2022.2093129.

[11] K. W. Jacobsen, J. K. Norskov, and M. J. Puska. "Interatomic interactions in the effective-medium theory". In: *Phys. Rev. B* 35 (14 May 1987), pp. 7423–7442. DOI: 10.1103/PhysRevB.35.7423. URL: https://link.aps.org/doi/10.1103/PhysRevB.35.7423.

[12] F. Murphy-Armando et al. "Electronic heat generation in semiconductors: Non-equilibrium excitation and evolution of zone-edge phonons via electron–phonon scattering in photo-excited germanium". In: *Applied Physics Letters* 122.1 (Jan. 2023), p. 012202. ISSN: 0003-6951. DOI: 10.1063/5.0131157. eprint: https://pubs.aip.org/aip/apl/article-pdf/doi/10.1063/5.0131157/16747519/012202_1_online.pdf. URL: https://doi.org/10.1063/5.0131157.

[13] K. P. Huber and G. Herzberg. "Constants of diatomic molecules". In: *Molecular Spectra and Molecular Structure: IV. Constants of Diatomic Molecules*. Boston, MA: Springer US, 1979, pp. 8–689. ISBN: 978-1-4757-0961-2. DOI: 10.1007/978-1-4757-0961-2_2. URL: https://doi.org/10.1007/978-1-4757-0961-2_2.

[14] William S. Benedict et al. "THE STRENGTHS, WIDTHS, AND SHAPES OF INFRARED LINES: II. THE HCl FUNDAMENTAL". In: *Canadian Journal of Physics* 34.8 (1956), pp. 850–875. DOI: 10.1139/p56-092. eprint: https://doi.org/10.1139/p56-092. URL: https://doi.org/10.1139/p56-092.

[15] Dario Alfè. "PHON: A program to calculate phonons using the small displacement method". In: *Computer Physics Communications* 180.12 (2009), pp. 2622–2633. ISSN: 0010-4655. DOI: https://doi.org/10.1016/j.cpc.2009.03.010. URL: https://www.sciencedirect.com/science/article/pii/S0010465509001064.

40 YEARS OF CPC: A celebratory issue focused on quality software for high performance, grid and novel computing architectures.

[16] Xiaoli Tang, Chen W. Li, and B. Fultz. "Anharmonicity-induced phonon broadening in aluminum at high temperatures". In: *Phys. Rev. B* 82 (18 Nov. 2010), p. 184301. DOI: 10.1103/PhysRevB.82.184301. URL: https://link.aps.org/doi/10.1103/PhysRevB.82.184301.

[17] R. Stedman and G. Nilsson. "Dispersion Relations for Phonons in Aluminum at 80 and 300°K". In: *Phys. Rev.* 145 (2 May 1966), pp. 492–500. DOI: 10.1103/PhysRev.145.492. URL: https://link.aps.org/doi/10.1103/PhysRev.145.492.